ACS APPLIED MATERIALS & INTERFACES

Research Article

Cite This: ACS Appl. Mater. Interfaces 2019, 11, 35404−35409

www.acsami.org

Scaled-up Direct-Current Generation in MoS_2 Multilayer-Based Moving Heterojunctions

Jun Liu,[†] Feifei Liu,[*,§] Rima Bao,[∥] Keren Jiang,[⊥] Faheem Khan,[⊥] Zhi Li,[⊥] Huihui Peng,[§] James Chen,[‡] Abdullah Alodhayb,[*,#] and Thomas Thundat[*,†]

[†]Department of Chemical and Biological Engineering and [‡]Department of Mechanical and Aerospace Engineering, University at Buffalo, The State University of New York, Buffalo, New York 14260, United States

[§]School of Electrical Engineering and Automation, Jiangxi University of Science and Technology, Ganzhou 341000, China

[∥]College of New Energy and Materials, China University of Petroleum, Beijing 102249, China

[⊥]Department of Chemical and Materials Engineering, University of Alberta, Edmonton, Alberta T6G 2V4, Canada

[#]Department of Physics and Astronomy, College of Science, King Saud University, Riyadh 11451, Saudi Arabia

ABSTRACT: Techniques for scaling-up the direct-current (dc) triboelectricity generation in MoS_2 multilayer-based Schottky nanocontacts are vital for exploiting the nanoscale phenomenon for real-world applications of energy harvesting and sensing. Here, we show that scaling-up the dc output can be realized by using various MoS_2 multilayer-based heterojunctions including metal/semiconductor (MS), metal/insulator (tens of nanometers)/semiconductor (MIS), and semiconductor/insulator (a few nanometers)/semiconductor (SIS) moving structures. It is shown that the tribo-excited energetic charge carriers can overcome the interfacial potential barrier by different mechanisms, such as thermionic emission, defect conduction, and quantum tunneling in the case of MS, MIS, and SIS moving structures. By tailoring the interface structure, it is possible to trigger electrical conduction resulting in optimized power output. We also show that the band bending in the surface-charged region of MoS_2 determines the direction of the dc power output. Our experimental results show that engineering the interface structure opens up new avenues for developing next-generation semiconductor-based mechanical energy conversion with high performance.

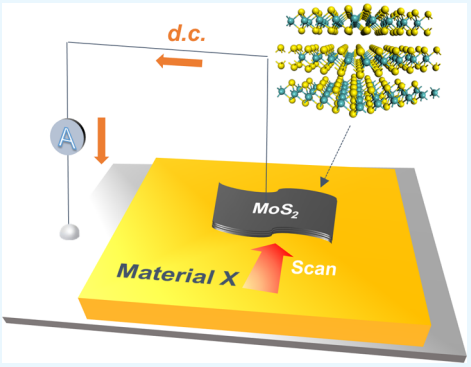

KEYWORDS: *energy harvesting, triboelectricity, tribo-tunneling, direct-current, heterojunction, MoS_2*

INTRODUCTION

Mechanical energy harvesting technologies such as triboelectric nanogenerator (TENG),[1−4] piezoelectric nanogenerator,[3] and electrochemical−mechanical generator[5,6] are promising for powering portable devices such as wearable/implantable electronics and sensor network and are critical to the future development of Internet of Things and smart medical care devices.[7,8] These energy harvesting concepts can also be applied as an electromechanical transducer for various chemical, biological, and physical motion sensing applications.[7,9] Among those energy harvesting techniques, direct-current (dc) generation at moving Schottky contacts is emerging as a new approach, which overcomes the current output limitation faced by traditional methods.[10−15] Specifically, Liu et al.[10] have demonstrated that the sliding of Pt/Ir-coated atomic force microscopy nanotip on a multilayered MoS_2 can generate ultrahigh dc current due to tribo-tunneling transport mechanism[11,12] and tribo-photovoltaic effect.[16] It has been proposed that the triboelectric charges can quantum mechanically tunnel through the thin forbidden barrier (surface oxide, 1−2 nm) in the metal/silicon (Si) tribo-tunneling system, thus generating sustained high current in the dc form.[11,12] However, scaling-up the MoS_2-based dc generation method remains as a challenge for practical applications. Here, it is shown that a MoS_2-based system can be scaled-up for dc current generation for practical applications. We also show that the triboelectric dc generation is a universal physical phenomenon at metal/insulator/semiconductor (MIS) and semiconductor/insulator/semiconductor (SIS) moving systems (Figure 1).

Two-dimensional transition-metal dichalcogenides such as MoS_2, $MoSe_2$, and WSe_2 are one of the most promising materials for future electronics, photonics, catalysis, sensing, and energy-storage applications.[17,18] The discovery of its out-of-plane piezoelectric property with few-layer structured (odd number: 1, 3, and 5 layers) MoS_2 initiated its applicability for mechanical energy harvesting[19−21] It is reported that a MoS_2 monolayer with 0.53% strain can generate peak outputs of 15 mW and 20 pA, corresponding to a power density of 2 mW/m^2.[21] Strong in-plane/out-plane piezoelectricity and flexoelec-

Received: June 5, 2019
Accepted: September 3, 2019
Published: September 3, 2019

DOI: 10.1021/acsami.9b09851
ACS Appl. Mater. Interfaces 2019, 11, 35404−35409

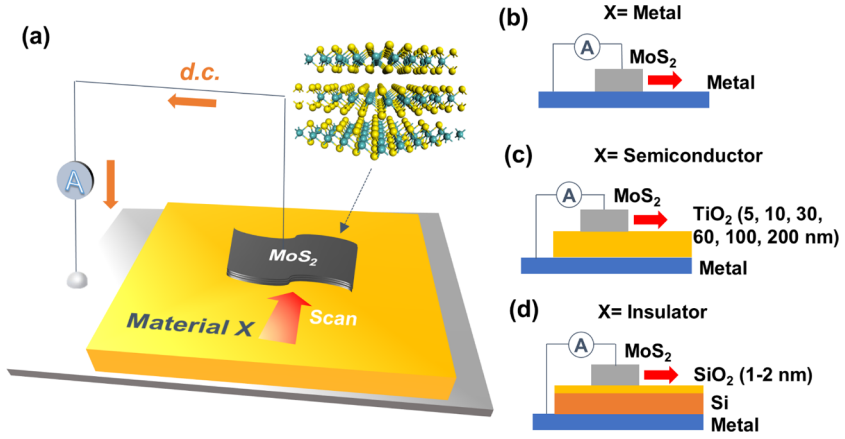

Figure 1. (a) Schematics of the MoS_2-based moving heterojunction as the direct-current generator. Interfacial electronic excitation can be induced by continuous friction between the MoS_2 multilayers and the contact material X. The surface charges are built up by thermionic emission and swept either by direct conduction or quantum-tunneling transport and thus generate dc current output. The contact material X can be (b) metal, (c) semiconductor, or (d) insulator.

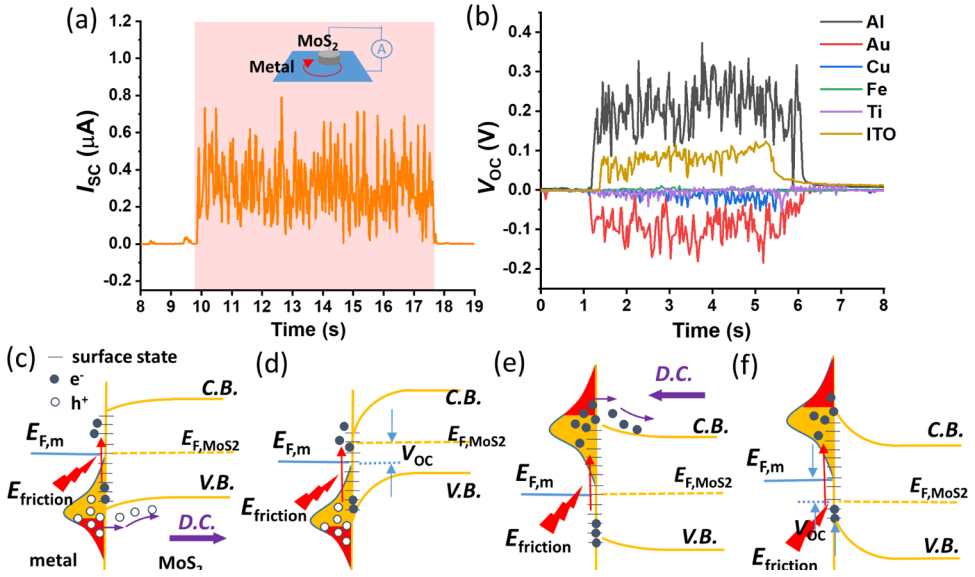

Figure 2. (a) Short-circuit current (I_{SC}) output in a MoS_2/Al moving junction. The MoS_2 is driven by a circular motion mode on the Al substrate. (b) Open-circuit voltage (V_{OC}) output in MoS_2/metal moving junctions with different metal substrates (Al, Au, Cu, Fe, Ti, and indium-tin oxide (ITO)). Band diagram of the cases with positive output (Al and ITO) under (c) short-circuit and (d) open-circuit conditions. Band diagram of the cases with negative output (Cu and Au) under (e) short-circuit and (f) open-circuit conditions. Basically, electronic excitation is induced at the frictional surface. Triboelectric charges are transferred via thermionic emission process, overcome the Schottky energy barrier, and get swept by the electric field in the semiconductor surface-charged region (SCR). The dc generation is completed by carrier conduction from the external circuit back to the metal substrate.

tricity are also predicted in the Janus monolayer and multilayer structures.[22,23] Meanwhile, a nanocomposite with MoS_2 monolayers inserted into the friction layer is proved to be an efficient way of improving the dielectric alternative current (ac) peak output of a polymer-based triboelectric nanogenerator (TENG) from 0.025 to 0.175 A/m^2.[24] In contrast, the dc generation in MoS_2-based moving heterojunctions works based on very different mechanisms compared to the piezoelectric or traditional electrostatic triboelectric generators.

RESULTS AND DISCUSSION

DC Generation in Metal/Semiconductor (MS) Moving Heterojunctions. The concept is demonstrated by sliding a piece of multilayered MoS_2 flake from a single crystal on different materials and recording the power output, as shown in Figure 1b. For example, MoS_2 when rubbed on an aluminum (Al) substrate under circular motion produces a sustained open-circuit voltage of V_{OC} of 0.3 V (Figure 2a) and short-circuit current of I_{SC} of 0.6 μA (Figure 1b). The current output corresponds to a current density J_{SC} of 0.35 A/m^2 (contact area $A \sim 1.7$ mm^2). It can be seen that the voltage and current output occurs simultaneously. Figure 2b shows that the V_{OC} output obtained with different metals. Negative outputs of −0.05 and −0.15 V are observed with Cu and Au, respectively, while the output is negligible with Ti and Fe. Here, the piezoelectric mechanism can be excluded since the piezoelectric output is found to decay rapidly when the layer number is larger than five and negligible in bulk MoS_2.[21] The mechanism is also fundamentally different from that in the polymer-based traditional TENGs: the dynamic voltage

DOI: 10.1021/acsami.9b09851
ACS Appl. Mater. Interfaces 2019, 11, 35404−35409

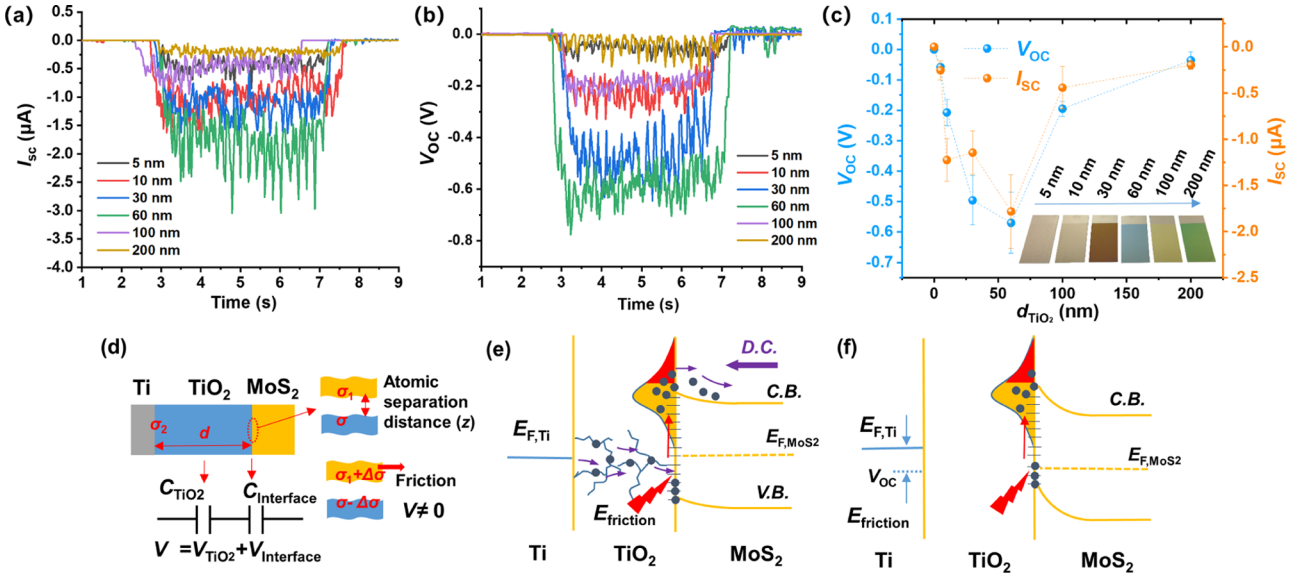

Figure 3. TiO_2 thickness (d_{TiO_2})-dependent (a) I_{SC} and (b) V_{OC} outputs in MoS_2/TiO_2 moving junctions. (c) Summaries of the analytic results of the d_{TiO_2}-dependent I_{SC} and V_{OC} data. Inset: the optical image of the TiO_2/Ti samples. (d) Schematics of the possible mechanism. The MoS_2/TiO_2 moving junction is simplified as two capacitors, C_{TiO_2} and $C_{interface}$, which are connected in parallel. C_{TiO_2} represents the dielectric capacitance of the TiO_2 thin film. The $C_{interface}$ corresponds to the atomic separation of the two contact bodies. Dynamic surface charge variation breaks the electronic equilibrium resulting in the V_{OC} in the dc transport. Band diagram of the MoS_2/TiO_2 moving junctions under (e) short-circuit and (f) open-circuit conditions. The carriers are conducted through the conducting paths (defect, grain boundaries, etc.) inside the e-beam-evaporated TiO_2 thin film.

generation at semiconductor-based moving junctions is related to a perturbed electronic interface rather than the capacitive voltage due to the separation of electrostatic charges, and the dc generation is the result exciting interfacial charge carrier and direct conduction through the junction instead of dielectric displacement alternating current (ac).[12]

The possible mechanism of metal/MoS_2 moving junction is proposed in Figure 2c–f: In the case of Al/MoS_2 junction, downward band bending may occur on MoS_2 surface-charged region (SCR) due to the relatively low work function Φ of Al (~4.2 eV).[25] When excited by frictional energy, energetic holes may undergo a thermionic emission process, overcome the interfacial Schottky energy barrier, and get swept by the electric field in the SCR generating the dc current (Figure 2c). Under open-circuit condition, the accumulated surface charges produce a dynamic surface potential difference, which corresponds to the V_{OC}. In contrast, metallic materials with relatively large Φ such as Au (~5.1 eV) would lead to an upward surface band bending, as shown in Figure 2e.[25] As a result, current and voltage directions have an opposite sign (Figure 2e,f). We shall also see that the metallic material can also be replaced by conducting oxide such ITO, as shown in Figure 2b. We notice that the surface pinning effect has been reported in the metal/MoS_2 static heterojunction structures resulting in a small Schottky energy barrier.[26−28] Compared to the chemical bond formation in the static MS structures where the metals are normally prepared by physical deposition methods, the interaction of surface atoms in the moving MS junction is more likely attributed to a relatively weak van der Waals force.[13] Therefore, it is proposed that the surface potential difference may still play a vital role in the metal-dependent output direction.

DC Generation in Metal/Insulator/Semiconductor (MIS) Moving Heterojunctions. The continuous dc output is also demonstrated using metal/insulator (thick)/semiconductor (MIS)-type of moving heterojunction. As shown in Figure 1c, TiO_2 thin film with different thicknesses (d_{TiO_2}) is deposited by e-beam evaporation on the Ti electrode/Si wafer. Ti thin film (50 nm) is deposited as the bottom electrode in advance. The I_{SC} and V_{OC} outputs vs. time in MoS_2/TiO_2 moving junctions are shown in Figure 3a,b, respectively. Negative voltage and current output are observed, which is in line with the cases of upward surface band bending, as discussed above. Figure 3c summarizes the d_{TiO_2}-dependent outputs. It can be seen that both the I_{SC} and V_{OC} output are maximum at d_{TiO_2} = 60 nm (V_{OC} of −0.7 V and I_{SC} of −2 μA J_{SC} = 1.2 A/m^2).

Here, it should be noted that the Ti/MoS_2 moving junction shows negligible output (Figure 2b), indicating that the observed dc output in MoS_2/TiO_2 moving junctions should be associated with the electronic properties on the TiO_2 surface rather than the Ti bottom material. According to the contact electrification theory, charge transfer takes place due to the overall potential difference between two contact bodies[29,30]

$$V = V_c + V_e \tag{1}$$

where V_c is considered to be the surface potential difference between two contact bodies and V_e is the image charge potential determined by the existing surface charges: $V_e = k_0 q$, where k_0 is a constant and q is the initial charge on the surface before contact. To explain the electrostatic charge accumulation in metal/dielectric/metal structures, Zhou et al.[31] developed the theory based on the parallel-plate model and Poisson equation

$$\sigma + \sigma_1 + \sigma_2 = 0 \tag{2}$$

$$\text{and} V = \frac{\sigma_1}{\varepsilon_0} z + \frac{\sigma_2}{\varepsilon_0 \varepsilon} t \tag{3}$$

DOI: 10.1021/acsami.9b09851
ACS Appl. Mater. Interfaces 2019, 11, 35404−35409

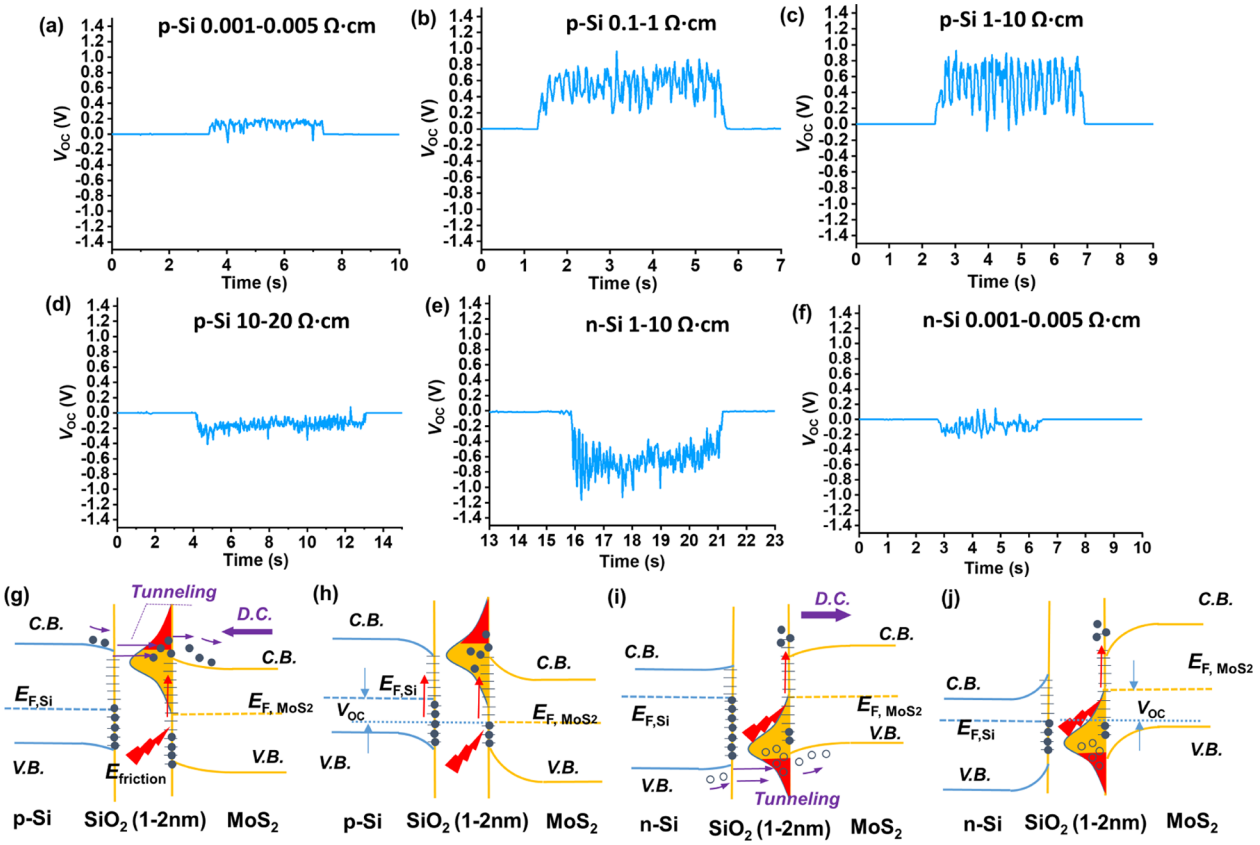

Figure 4. V_{OC} output in Si/MoS_2 moving junction (a) p-Si 0.001−0.005 Ω cm, (b) p-Si 0.1−1 Ω cm, (c) p-Si 1−10 Ω cm, (d) p-Si 10−20 Ω cm. (e) n-Si 1−10 Ω cm, and (f) n-Si 0.001−0.005 Ω cm. Band diagram of the p-type Si/MoS_2 junction under (g) short-circuit and (h) open-circuit conditions; n-type Si/MoS_2 junction under (i) short-circuit and (j) open-circuit conditions. Friction-excited carriers can quantum mechanically tunnel through the ultrathin SiO_2 layer and get swept by the electric field in the SCR.

where σ, σ_1, and σ_2 are the dielectric surface charge, induced charge on the top metal, and the induced charge on the bottom metal, respectively. V is the potential difference between the top and bottom metal electrodes. z denotes the separation distance between the two contact bodies (a metal and a dielectric), which is on the range of a few angstroms. t and ε represent the thickness and the dielectric constant of the dielectric materials. ε is the vacuum permittivity. Here, $V = 0$, when the top electrode is in intimate contact with the dielectric.[7] Under lateral friction, however, one would expect a dynamic variation of interfacial charge $\Delta\sigma$ due to the nonequilibrium surface potential difference along with a nonadiabatic electronic excitation (Figure 3d).[12] As a result, the balance of V in eq 3 will be perturbed, which ascribes that the nonequilibrium V_{OC} output is a MoS_2/TiO_2/Ti moving structure

$$V_{OC} = \Delta V = \frac{\sigma_1 + \Delta\sigma}{\varepsilon_0} z + \frac{\sigma_2}{\varepsilon_0 \varepsilon} t \quad (4)$$

However, the ΔV will diminish immediately once the friction stops, as the image charge σ_2 will promptly respond to the $\Delta\sigma$ and rebuild the electrostatic equilibrium (i.e., $V = 0$). As we have shown above, the negligible power output in the Ti/MoS_2 moving system indicates that surface potentials of Ti and MoS_2 are very close to each other. As the d_{TiO_2} increases in the very beginning, the surface potential level of TiO_2 (E_0) may deviate from the $E_{F,Ti}$, which results in larger $\Delta\sigma$ and contributes to the increased V_{OC} output. On the other hand, it is evident that further increasing the dielectric layer thickness will lead to a smaller $\Delta\sigma$ in the two-capacitor model.[31] The thick dielectric layer should also increase the internal resistance of the generator. Therefore, an optimal d_{TiO_2} may exist, as revealed by the experimental results.

We shall now discuss about the dc conduction mechanism in the MoS_2/TiO_2/Ti moving structure. It is proposed that the e-beam-evaporated TiO_2 thin film contains a large number of conducting paths (defect, grain boundaries, etc.), which allows the conduction of friction-excited carriers through them.[32] In the case of a compact dielectric thin film such as the atomic layer-deposited SiO_2, such conducting mechanism fails since the thin film would have an excellent insulating property. However, quantum mechanical tunneling mechanism may exist when this dielectric layer is extremely thin (<2 nm).[11]

DC Generation in Semiconductor/Insulator/Semiconductor (SIS) Moving Heterojunctions. Earlier, we have reported on the current generation due to quantum-tunneling mechanism in a MIS moving structure.[11,12] Here, it is shown that the semiconductor/insulator/semiconductor (SIS) moving structure can also give rise to the tribo-tunneling dc power output. Figure 4a−f shows the V_{OC} output of the Si/SiO_2/MoS_2 moving junction with different Si doping types/concentrations (University Wafer, Inc.). It can be seen that a positive V_{OC} output is measured with p-Si 0.001−0.005 Ω cm, p-Si 0.1−1 Ω cm, and p-Si 1−10 Ω cm samples, while a negative V_{OC} output is obtained with p-Si 10−20 Ω cm, n-Si 1−10 Ω cm, and n-Si 0.001−0.005 Ω cm samples. It is

DOI: 10.1021/acsami.9b09851
ACS Appl. Mater. Interfaces 2019, 11, 35404−35409

suggested that the surface potential of the Si samples may induce different surface band bendings of MoS_2. In the case of a p-type Si/MoS_2 junction, an upward surface band bending may be induced in MoS_2. (Figure 4g) Friction-excited electrons can quantum mechanically tunnel through the ultrathin SiO_2 layer and get swept by the electric field in the SCR, which accounts for the dc output in a positive direction. (Figure 4h) On the other hand, the downward band bending in a n-type Si/MoS_2 junction may result in the hole tunneling and conduction in the negative direction generating the dc output. (Figure 4i–j) In our previous work, the insensitivity of Si doping type/concentration on the power output direction is found in metal/Si moving contact systems.[12] It is proved by Kelvin probe force microscopy that the surface potential of a wide range of p-/n-type Si samples is similar, which may be due to the fermi-level pinning due to the surface states or surface dipole effect via air molecular adsorption.[12] We also demonstrated in the HF etching experiment that the surface oxide plays an important role in the surface state formation on the Si surface.[12] Therefore, it is proposed that the similar output characteristics on the p-Si (10–20 Ω cm) and the n-Si samples may be attributed to the surface Fermi-level pinning of the Si surface due to the existence of surface oxide and/or defects. We shall also see that the heavily doped n-/p-type Si samples (degenerated) exhibit a much lower power output.

CONCLUSIONS

In summary, dc power output with high current density has been proved in MoS_2 multilayer-based moving heterojunctions with various structures (i.e., MS, MIS, and SIS). It is proposed that the dc conduction mechanism is thermionic emission, defect conduction, and quantum tunneling of the tribo-excited energetic carriers in the case of MS, MIS, SIS systems, respectively. It is shown that the surface band bending of MoS_2 in contact with another material plays a key role in determining the direction of power output. We found that by adding the interfacial dielectric layer with different thicknesses, the voltage and current output can be manipulated. It is expected that the triboelectric dc power output can be further enhanced by interface engineering such as using high K dielectric materials, polymer/inorganic nanocomposite, and metal/inorganic nanocomposite. The excellent lubricant properties of the layered materials endow them with a promising future in triboelectric dc nanogenerators. It also opens new avenues for exploring all kinds of semiconductor-based moving heterojunction for dc-based energy harvesting and sensing applications.

METHODS

TiO_2 Sample Preparation. To deposit titanium oxide on silicon (Si) wafers, the standard 4 in. wafers were diced into 25 mm × 50 mm rectangular substrates. After dicing, the rectangular Si substrates were rinsed water and then ethanol, followed by drying with nitrogen. In total, 24 substrates were prepared. Then, a set of four substrates was loaded in the vacuum chamber of the electron beam evaporation system (Kurt J. Lesker). For all of the substrates, 50 nm titanium was deposited at a vacuum level of 1.5×10^{-6} mTorr and a deposition rate of 0.8 Å/s. After that a portion of 10 mm × 25 mm of each substrate was covered with the Kapton tape, to use that for a later formation of an electrode. Then, the substrates were loaded again in the deposition chamber to separately deposit 5, 10, 30, 60, 100, and 200 nm on the sets of four substrates. The deposition was performed on the area of 25 mm × 40 mm at a vacuum level of 2×10^{-6} mTorr and a deposition rate of between 0.6 and 1.1 Å/s.

Triboelectric dc Power Measurement. MoS_2 single crystal was purchased from SPI Supplies. The Si wafers with different doping type/concentration were purchased from University Wafer, LNC. and coated with Al thin film (200 nm) as the bottom electrode. The current and voltage output is measured by a Keithley DMM6500 6-1/2 Digi Multimeter. The $I-V$ curve is characterized by a Keithley 2450 Source Measurement Unit. The speed and force are controlled by a customized automatic motor system.

AUTHOR INFORMATION

Corresponding Authors

*E-mail: gzlff@126.com (F.L.).
*E-mail: aalodhayb@ksu.edu.sa (A.A.).
*E-mail: tgthunda@buffalo.edu (T.T.).

ORCID

Keren Jiang: 0000-0001-6389-9875
Abdullah Alodhayb: 0000-0003-0202-8712
Thomas Thundat: 0000-0003-1721-1181

Notes

The authors declare no competing financial interest.

ACKNOWLEDGMENTS

J.L. and T.T. acknowledge funding support from the University at Buffalo and RENEW Institute. J.C. gratefully acknowledges the support from the U.S. National Science Foundation (grant number 1662879) for this research.

REFERENCES

(1) Wu, C.; Wang, A. C.; Ding, W.; Guo, H.; Wang, Z. L. Triboelectric Nanogenerator: A Foundation of the Energy for the New Era. *Adv. Energy Mater.* **2019**, *9*, No. 1802906.
(2) Chen, B.; Yang, Y.; Wang, Z. L. Scavenging Wind Energy by Triboelectric Nanogenerators. *Adv. Energy Mater.* **2018**, *8*, No. 1702649.
(3) Askari, H.; Khajepour, A.; Khamesee, M. B.; Saadatnia, Z.; Wang, Z. L. Piezoelectric and Triboelectric Nanogenerators: Trends and Impacts. *Nano Today* **2018**, *22*, 10–13.
(4) Wang, Z. L.; Jiang, T.; Xu, L. Toward the Blue Energy Dream by Triboelectric Nanogenerator Networks. *Nano Energy* **2017**, *39*, 9–23.
(5) Kim, S.; Choi, S. J.; Zhao, K.; Yang, H.; Gobbi, G.; Zhang, S.; Li, J. Electrochemically Driven Mechanical Energy Harvesting. *Nat. Commun.* **2016**, *7*, No. 10146.
(6) Kim, S. H.; Haines, C. S.; Li, N.; Kim, K. J.; Mun, T. J.; Choi, C.; Di, J.; Oh, Y. J.; Oviedo, J. P.; Bykova, J.; et al. Harvesting Electrical Energy from Carbon Nanotube Yarn Twist. *Science* **2017**, *357*, 773–778.
(7) Wang, Z. L. Triboelectric Nanogenerators as New Energy Technology for Self-Powered Systems and as Active Mechanical and Chemical Sensors. *ACS Nano* **2013**, *7*, 9533–9557.
(8) Wang, Z. L. Triboelectric Nanogenerators as New Energy Technology and Self-Powered Sensors–Principles, Problems and Perspectives. *Faraday Discuss.* **2015**, *176*, 447–458.
(9) Zhu, G.; Peng, B.; Chen, J.; Jing, Q.; Wang, Z. L. Triboelectric Nanogenerators as a New Energy Technology: From Fundamentals, Devices, to Applications. *Nano Energy* **2015**, *14*, 126–138.
(10) Liu, J.; Goswami, A.; Jiang, K.; Khan, F.; Kim, S.; McGee, R.; Li, Z.; Hu, Z.; Lee, J.; Thundat, T. Direct-Current Triboelectricity Generation by a Sliding Schottky Nanocontact on Mos_2 Multilayers. *Nat. Nanotechnol.* **2018**, *13*, No. 112.
(11) Liu, J.; Miao, M.; Jiang, K.; Khan, F.; Goswami, A.; McGee, R.; Li, Z.; Nguyen, L.; Hu, Z.; Lee, J.; et al. Sustained Electron Tunneling at Unbiased Metal-Insulator-Semiconductor Triboelectric Contacts. *Nano Energy* **2018**, *48*, 320–326.
(12) Liu, J.; Jiang, K.; Nguyen, L.; Li, Z.; Thundat, T. Interfacial Friction-Induced Electronic Excitation Mechanism for Tribo-Tunneling Current Generation. *Mater. Horiz.* **2019**, *6*, 1020–1026.

DOI: 10.1021/acsami.9b09851
ACS Appl. Mater. Interfaces 2019, 11, 35404–35409

(13) Lin, S.; Lu, Y.; Feng, S.; Hao, Z.; Yan, Y. A High Current Density Direct-Current Generator Based on a Moving Van Der Waals Schottky Diode. *Adv. Mater.* **2018**, No. 1804398.
(14) Shao, H.; Fang, J.; Wang, H.; Zhou, H.; Niu, H.; Chen, F.; Yan, G.; Fu, S.; Cao, Y.; Lin, T. Doping Effect on Conducting Polymer-Metal Schottky Dc Generators. *Adv. Electron. Mater.* **2018**, No. 1800675.
(15) Shao, H.; Fang, J.; Wang, H.; Dai, L.; Lin, T. Polymer−Metal Schottky Contact with Direct-Current Outputs. *Adv. Mater.* **2016**, *28*, 1461−1466.
(16) Liu, J.; Zhang, Y.; Chen, J.; Bao, R.; Jiang, K.; Khan, F.; Goswami, A.; Li, Z.; Liu, F.; Feng, K. Separation and Quantum Tunneling of Photo-Generated Carriers Using a Tribo-Induced Field. *Matter* **2019**, *1*, 650−660.
(17) Chhowalla, M.; Liu, Z.; Zhang, H. Two-Dimensional Transition Metal Dichalcogenide (Tmd) Nanosheets. *Chem. Soc. Rev.* **2015**, *44*, 2584−2586.
(18) Manzeli, S.; Ovchinnikov, D.; Pasquier, D.; Yazyev, O. V.; Kis, A. 2d Transition Metal Dichalcogenides. *Nat. Rev. Mater.* **2017**, *2*, No. 17033.
(19) Wu, W.; Wang, L.; Yu, R.; Liu, Y.; Wei, S. H.; Hone, J.; Wang, Z. L. Piezophototronic Effect in Single-Atomic-Layer Mos2 for Strain-Gated Flexible Optoelectronics. *Adv. Mater.* **2016**, *28*, 8463−8468.
(20) Zhou, Y.; Liu, W.; Huang, X.; Zhang, A.; Zhang, Y.; Wang, Z. L. Theoretical Study on Two-Dimensional Mos 2 Piezoelectric Nanogenerators. *Nano Res.* **2016**, *9*, 800−807.
(21) Wu, W.; Wang, L.; Li, Y.; Zhang, F.; Lin, L.; Niu, S.; Chenet, D.; Zhang, X.; Hao, Y.; Heinz, T. F. Piezoelectricity of Single-Atomic-Layer Mos 2 for Energy Conversion and Piezotronics. *Nature* **2014**, *514*, No. 470.
(22) Cai, H.; Guo, Y.; Gao, H.; Guo, W. Tribo-Piezoelectricity in Janus Transition Metal Dichalcogenide Bilayers: A First-Principles Study. *Nano Energy* **2019**, *56*, 33−39.
(23) Shi, W.; Guo, Y.; Zhang, Z.; Guo, W. Flexoelectricity in Monolayer Transition Metal Dichalcogenides. *J. Phys. Chem. Lett.* **2018**, *9*, 6841−6846.
(24) Wu, C.; Kim, T. W.; Park, J. H.; An, H.; Shao, J.; Chen, X.; Wang, Z. L. Enhanced Triboelectric Nanogenerators Based on Mos2 Monolayer Nanocomposites Acting as Electron-Acceptor Layers. *ACS Nano* **2017**, *11*, 8356−8363.
(25) Hölzl, J.; Schulte, F. K. Work Function of Metals. In *Solid Surface Physics*; Springer, 1979; pp 1−150.
(26) Kim, C.; Moon, I.; Lee, D.; Choi, M. S.; Ahmed, F.; Nam, S.; Cho, Y.; Shin, H.-J.; Park, S.; Yoo, W. J. Fermi Level Pinning at Electrical Metal Contacts of Monolayer Molybdenum Dichalcogenides. *ACS Nano* **2017**, *11*, 1588−1596.
(27) Kim, G.-S.; Kim, S.-H.; Park, J.; Han, K. H.; Kim, J.; Yu, H.-Y. Schottky Barrier Height Engineering for Electrical Contacts of Multilayered Mos2 Transistors with Reduction of Metal-Induced Gap States. *ACS Nano* **2018**, *12*, 6292−6300.
(28) Kim, S.-H.; Han, K. H.; Kim, G.-S.; Kim, S.-G.; Kim, J.; Yu, H.-Y. Schottky Barrier Height Modulation Using Interface Characteristics of Mos2 Interlayer for Contact Structure. *ACS Appl. Mater. Interfaces* **2019**, *11*, 6230−6237.
(29) Matsusaka, S.; Ghadiri, M.; Masuda, H. Electrification of an Elastic Sphere by Repeated Impacts on a Metal Plate. *J. Phys. D: Appl. Phys.* **2000**, *33*, No. 2311.
(30) Zhou, Y. S.; Liu, Y.; Zhu, G.; Lin, Z.-H.; Pan, C.; Jing, Q.; Wang, Z. L. In Situ Quantitative Study of Nanoscale Triboelectrification and Patterning. *Nano Lett.* **2013**, *13*, 2771−2776.
(31) Zhou, Y. S.; Wang, S.; Yang, Y.; Zhu, G.; Niu, S.; Lin, Z.-H.; Liu, Y.; Wang, Z. L. Manipulating Nanoscale Contact Electrification by an Applied Electric Field. *Nano Lett.* **2014**, *14*, 1567−1572.
(32) Chiu, F.-C. A Review on Conduction Mechanisms in Dielectric Films. *Adv. Mater. Sci. Eng.* **2014**, *2014*, No. 578168.

DOI: 10.1021/acsami.9b09851
ACS Appl. Mater. Interfaces 2019, 11, 35404−35409